Experimental detection of forming limit strains on samples with multiple local necks

Dmitry Vysochinskiy[a], Terence Coudert[b], Odd Sture Hopperstad[a], Odd-Geir Lademo[b,a], Aase Reyes[a,1]

[a] *Department of Structural Engineering, Norwegian University of Science and Technology Richard Birkelands vei 1A, Trondheim, N-7491 , Norway*
[b] *Department of Material- and Structural Mechanics, SINTEF Materials and Chemistry Richard Birkelands vei 2B, Trondheim, N-7491 , Norway*

Abstract

Sheet metal formability is traditionally described by the Forming Limit Curve (FLC). Experimental FLCs are obtained by performing formability tests and determining failure strains. The strains are usually measured either by etching a grid on the sheet surface or by Digital Image Correlation (DIC). Ductile metal sheets fail primarily by local necking which introduces a severe strain gradient in the failure region. This makes accurate detection of the failure strains challenging. An international standard (ISO 12004-2:2008) was introduced in 2008 to unify the procedure of FLC detection, prior to this large discrepancies were observed between the results reported by different laboratories. The main limitation of the standard method for detection of forming limits is that its application is limited to cases where a single local neck is formed in the metal sheet prior to fracture. In the case of multiple local necks, the samples are simply discarded. Furthermore, the standard method does not include any guidelines to distinguish the failure by local necking and direct failure by fracture. One of the advantages of DIC over the traditional etched-grid technique is that the former allows us to obtain not only the strain distribution but also its history. This allows for alternative methods for detection of forming limit strains. This paper introduces a DIC-based method which was specially developed to handle

[1] Corresponding author aase.reyes@ntnu.no

the case of multiple local necks and to distinguish failure by local necking from direct fracture automatically. The method is not confined to a single test type and can be used in combination with different formability tests as long at DIC is used to measure strains.
Keywords: Forming Limit Curve, Forming Limit Diagram, formability, sheet metal, Digital Image Correlation, local necking

---

1. Introduction

As stated by Hosford & Caddell (2007), the invention of the Forming Limit Diagram (FLD) by Keeler (1968) and Goodwin (1968) has literally transformed the field of sheet metal forming from art into science. Since then sheet metal formability is commonly described by FLDs that provide a quantitative description. The traditional FLD is a diagram with major and minor strains on its axes with a line dividing safe levels of strains from unsafe ones denoted as the Forming Limit Curve (FLC). The lowest point of the FLC lies near the plane-strain state and is denoted as FLD_0.

One of the challenges connected to the use of the FLC for description of formability is the accurate measurement of the failure strains. Since ductile metal sheets typically fail by formation of a local neck, large discrepancies in the measured strains can be observed depending on how far from the neck the measurements have been taken. Liebertz et al. (2004) reported a round robin formability test series on the same material performed by three different laboratories that produced $FLD_0 \approx 0.15$, $FLD_0 \approx 0.21$ and $FLD_0 \approx 0.25$ respectively. In order to prevent such discrepancies Liebertz et al. (2004) developed a set of guidelines for detection of the forming limit strains. In a second round robin the guidelines were implemented and the different laboratories produced similar results. These guidelines served as foundation for the international standard ISO12004-2:2008 (2008) and this method for detection of the forming limit strains is referred to as the *standard method* further in the text.

In the standard method, the forming limit strains are detected by fitting

an inverse parabola to the strain distribution in the vicinity of the fracture line. Thus, the method relies on the formation of a single local neck prior to fracture to ensure a good fit. The international standard ISO12004-2:2008 (2008) explicitly states that samples with multiple local necks shall be discarded.

The experience accumulated over several years of the use of the standard method showed that the method might not be applicable to some types of metallic materials. As reported by Hotz et al. (2013), some high-strength steels and aluminium alloys show non-homogeneous deformation behaviour providing no reasonable fit for the inverse parabola. This leads to an invalid mathematical evaluation if the standard method is used. In order to evaluate the formability of such alloys an alternative method is needed.

The development of the Digital Image Correlation (DIC) technique for strain measurements provides new opportunities for the detection of limit strains. DIC is a technique used to determine the displacements of a surface from the analysis of its images. Since the pictures are taken continuously through the test, the technique produces the displacement history as well. Providing sufficient accuracy, the strain fields can be calculated from the displacement fields. DIC techniques can be classified into 2D-DIC and 3D-DIC. 2D-DIC utilizes a single camera and is limited to in-plane deformations of flat surfaces. 3D-DIC allows for handling surfaces that deform out of their original plane. This technique utilizes two cameras and produces a three-dimensional displacement field. 3D-DIC produces the surface topography along with the surface strains.

The onset of local necking corresponds to an increase in the local strain rate. Marron et al. (1997) were the first to suggest using the evolution of strain rate to detect the onset of local necking. They used a combination of a circular grid and cameras to record the strain evolution. Later Merklein et al. (2010) independently implemented a method based on similar principles using DIC. The common feature of the strain-rate based methods is that the plot of strain-rate vs. time for a region affected by the local neck is used to determine the onset of local necking. The main difference between the methods used by different authors is the mathematical algorithm adopted. Marron et al. (1997)

proposed to use an intersection of two straight lines fitted to the major strain rate evolution: one before the increase in the strain rate and one after. Merklein et al. (2010) used the time derivative of the major strain rate in combination with an original algorithm. Situ et al. (2011) detected the onset of local necking at the maximum value of the time derivative of the major strain rate. Vysochinskiy et al. (2012) used an original algorithm based on the analysis of the major strain rate itself and detected onset of necking at the point of greatest curvature of the strain rate plot. Volk & Hora (2011) utilized the same algorithm as Marron et al. (1997) but applied it to the the strain-rate in the thickness direction $\dot{\epsilon}_3$, instead of the major strain rate $\dot{\epsilon}_1$. Hotz et al. (2013) presented a comparison of the algorithms proposed by Merklein et al. (2010) and Volk & Hora (2011) and two new algorithms. Hora et al. (2012) linked the local strain rate to the level of strain localization replacing the traditional FLD with the Localisation Level FLD (LL-FLD). This approach produces several FLCs that correspond to different levels of localization and is thus similar to the Forming Limit Band approach proposed by Janssens et al. (2001).

The strain-rate based methods for detection of forming limits are not yet standardized and there is no commonly accepted algorithm. Use of different algorithms leads to different results, which can be either more or less conservative than the ones obtained by the standard method. For example, in the comparison presented by Hotz et al. (2013) one of the analysed methods is more and three are less conservative than the standard. In addition, a drawback of the strain-rate based methods is that calculation of the rate amplifies the noise naturally present in the DIC strain measurements. Thus, these methods require the noise in the measurements to be low, otherwise smoothing of the strain evolution curve may be needed. Smoothing in itself is an additional procedure that may affect the results.

Some DIC-based methods do not utilize the strain rate history. Vacher et al. (1999b) suggested to use the strain velocity map between two subsequent images in the DIC analysis to determine when the strain field is no longer homogeneous. The onset of local necking is detected when a strain gradient above certain

tolerance level is observed. This method is limited to the case of homogeneous deformation. Wang et al. (2014) utilized the surface topography produced by the 3D-DIC software to detect the onset of local necking. They compared the surface height of a point inside and a point outside the neck to determine the onset of local necking. This method is limited to the flat surfaces provided by the flat punch in Marciniak-Kuczynski formability tests.

In this paper a new robust and user-independent method for detection of forming limit strains is proposed. The method was developed to enable detection of forming limits in AA6016 aluminium alloy sheets that displayed non-homogeneous deformation in biaxial tension. Thus, the method was designed to handle the case of multiple local necks that is not covered by the international standard ISO12004-2:2008 (2008). The method does not require calculation of the strain rate and is thus more robust with respect to noise in comparison with the strain-rate based methods. The detection of the forming limit strains can be fully automated and input parameters and any influence from the user are explicitly specified to ensure that different users would obtain the same result when using the proposed method.

2. Material and experimental program

The investigated material is aluminium alloy AA6016 commonly used in the car-body due to its good forming properties. The investigated sheets have nominal thickness 1.5 mm and are intended for the manufacturing of some inner parts of the car body. Thus, there are no surface quality requirements.

This paper covers the formability tests on as-received AA6016 sheets which are a part of a larger experimental programme intended to characterize the material properties (Vysochinskiy, 2014). The experimentally obtained true stress-strain curve for this material is illustrated in Fig. 1. The formability tests were performed in a BUP600 forming machine. The test set-up is illustrated in Fig. 2.

The intention was to characterize the formability of the material and con-

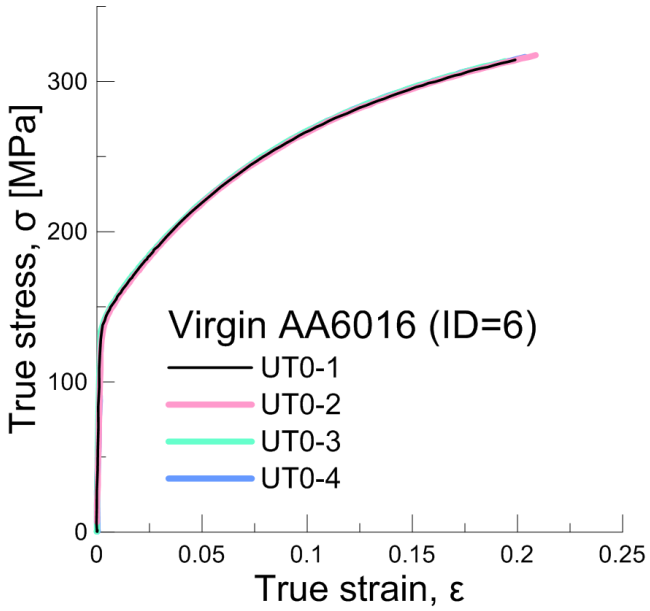

Figure 1: True stress-strain curves from uniaxial tension tests of virgin AA6016 samples (Vysochinskiy, 2014)

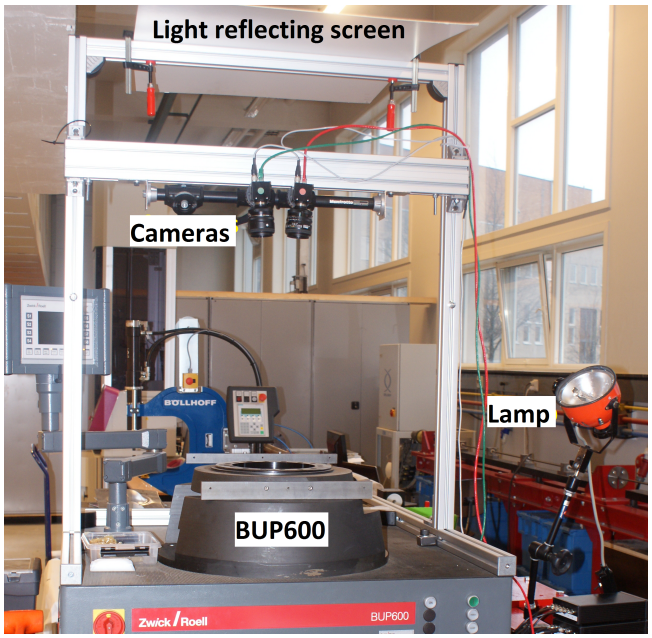

Figure 2: Formability test set-up

struct the FLC in biaxial tension through Marciniak-Kuczynski tests (Marciniak & Kuczynski, 1967). In this type of test a sheet of metal is stretched over a flat punch with an underlying blank with a hole that creates a friction-free zone in the middle. Rectangular 205 mm long samples were used. To achieve different strain-paths, different widths: 155 mm, 160 mm, 165 mm and 205 mm were used. Since the material is expected to be anisotropic, samples with their long side oriented both parallel and normal to the rolling direction were used. Hence, sample labels such as MK165-0-x and MK165-90-x were used,where 165 denotes sample width in mm, 0 or 90 denotes an angle in degrees between sample axis and rolling direction, and the last digit is a sample number to distinguish duplicate tests. For the square 205x205 mm samples the angle notation is redundant and these samples were marked simply as MK205-x. Two duplicate tests were performed for each strain path with the exception of equibiaxial tension (MK205 samples), where four duplicate tests were executed.

In addition to Marciniak-Kuczynski tests, several Nakajima formability tests (Nakajima et al., 1968) were performed. These tests were carried out using the same set-up but with a spherical punch. Lubrication in form of 0.1 mm thick Teflon sheets and grease was used to minimize the friction. Most Nakajima samples fractured in the clamping zone; there was only one sample geometry that produced three successful duplicate tests. This sample geometry was denoted as NK0-100 and provided a strain path between uniaxial and plane strain tension. The sample geometry is illustrated in Fig. 3. NK0-100 samples had their axes oriented normal to the rolling direction, 0 in the sample name denotes an angle in degrees between sample axis and the outer blank axis, while 100 refers to the facet radius in mm.

The surface of the sample was painted with a random black-and-white pattern for DIC measurements. In addition, the initial friction-free zone as well as the rolling direction were marked on the top of the sheet. This is visible in Fig. 4 that illustrates a Marciniak-Kuczynski sample in the machine prior to testing. Fig. 5 shows the samples and the underlying blanks after the test.

The punch velocity was set to 0.3 mm/s. The deformation process was filmed

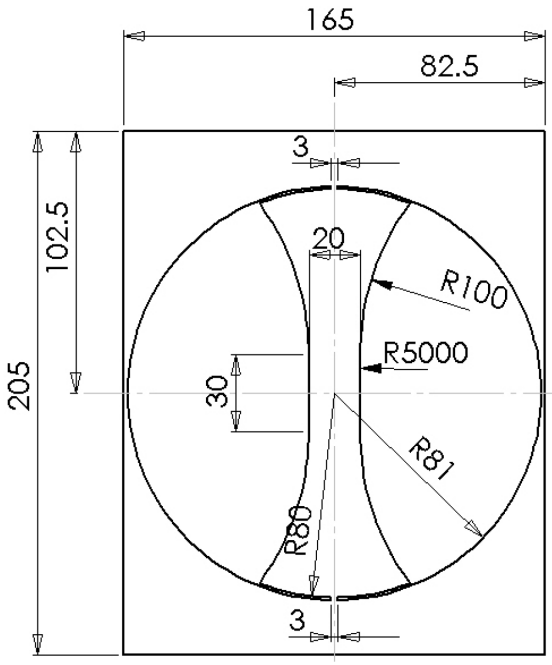

Figure 3: Geometry of the NK0-100 sample

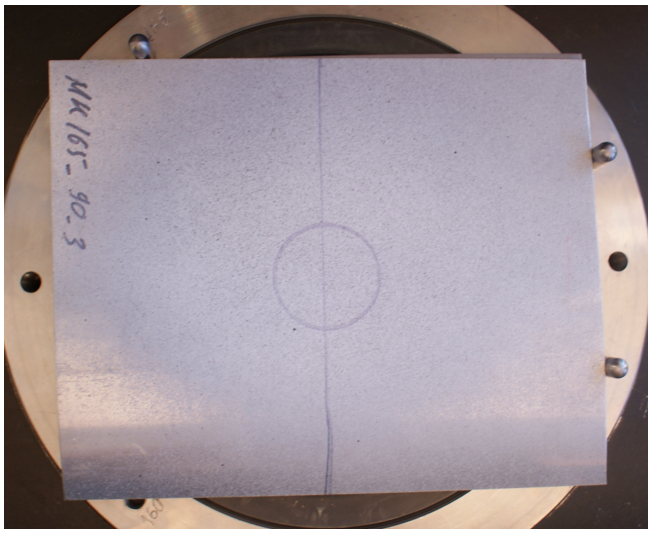

Figure 4: A Marciniak-Kuczynski sample in the machine

by two Procilica cameras visible in Fig. 2 with a frame frequency of 4 Hz. The 7D software (Vacher et al., 1999a) was used to perform DIC analysis of the images to determine strains. The DIC analysis was performed up until, but not including, the image where fracture appears visible on the sheet surface. For the Marciniak-Kuczynski samples the analysis area was set equal to the initial friction-free zone marked on the surface.

3. Initial results

The examination of the fractured samples as well as the results of the DIC-analysis showed that the tested material demonstrates different behaviour prior to fracture depending on the imposed strain path. Three different samples, i.e. NK0-100-1, MK205-4 and MK165-0-2, are chosen as examples and are followed through further in the text to illustrate different aspects of the behaviour of the tested AA6016 sheets.

The Nakajima test samples failed by formation of a single crack as Fig. 6(a) illustrates. The strain map obtained by DIC analysis depicted in Fig. 6(b) confirms that a single local neck was formed prior to fracture. Thus, these

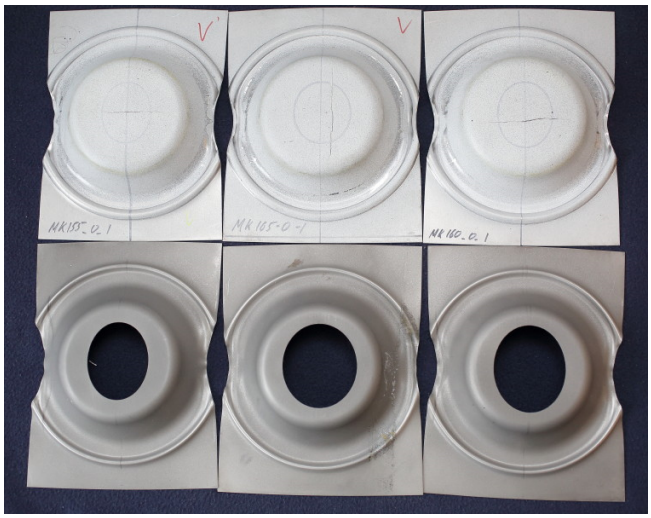

Figure 5: Marciniak-Kuczynski samples after the test

samples provide a good fit for the application of the standard cross-section method. The application of this method is illustrated in Fig. 6. The strain field for the last image before fracture is analysed. First, a line is drawn along the anticipated fracture direction. Second, five cross-sectional lines are drawn normal to the fracture line as Fig. 6(b) illustrates. Third, the strain distribution along each cross-section is plotted, fitting windows are determined according to the standard, an inverse parabola is fitted, and the forming limit strain is determined at its apex. For the middle cross-section of the NK0-100-1 sample, the strain distribution, the fitted parabola and the detected forming limit strain are illustrated in Fig. 6(c).

For the Marciniak-Kuczynski tests the situation is different. Some samples, like MK205-4 illustrated in Fig. 7, failed by forming a single crack in the middle. In this case application of the standard method is still possible, but the provided fit is rather different from the Nakajima samples, as Fig. 7(c) illustrates. Furthermore, the strain field contains secondary strain localizations, as observed in Fig. 7(b). If these strain localizations are regarded as multiple necks, this sample needs to be discarded according to the standard.

For some other samples, like MK165-0-2, the fracture forms a zig-zag pattern, as illustrated in Fig. 8(a). An examination of the strain map in Fig. 8(b) reveals that the fracture line follows the pattern of multiple local necks formed in the sample. For this sample there is no good fit for the inverse parabola (see Fig. 8(c)).

Another interesting aspect of the behaviour of the MK0-165 samples is that fracture was oriented parallel to the major strain axis, which is counter-intuitive. This can seen in Fig. 8(a) as the orientation of the major strain axis can be determined from the shape of the initially round friction-free zone.

A closer examination of the specimens revealed that the multiple strain localizations observed for AA6016 in biaxial tension are likely to be connected to the roping phenomenon. Roping (also called ridging) is a tendency of groups of metal grains to deform together and form a rope-like structures (ridges) on the sheet surface, hence the name roping (ridging). According to Engler et al. (2012), roping is a common phenomenon for aluminium alloys like AA6016.

Fig. 9 illustrates a bottom view of a tested Marciniak-Kuczynski sample of AA6016 where roping and multiple local necks are visible. An arrow marks the rolling direction. The presence of roping explains the anomalous orientation of the fracture lines in the MK0-165 samples: local necking and subsequent fracture simply follow the orientation of the roping, which is in the rolling direction, as Fig. 9 indicates.

As the investigated material is intended for the inner parts of the car body, there are no requirements to surface quality, and surface roughening due to roping is not considered to be a problem. However, the phenomenon makes the deformation inhomogeneous and promotes multiple local necks. Hence, the tested AA6016 belongs to the type of materials mentioned by Hotz et al. (2013), i.e. the materials that undergo inhomogeneous deformation and provide no good fit for the standard method.

The international standard ISO12004-2:2008 (2008) explicitly requires to discard test samples that display multiple local necks while for the alternative strain-rate based methods no commonly accepted algorithm exists. Therefore,

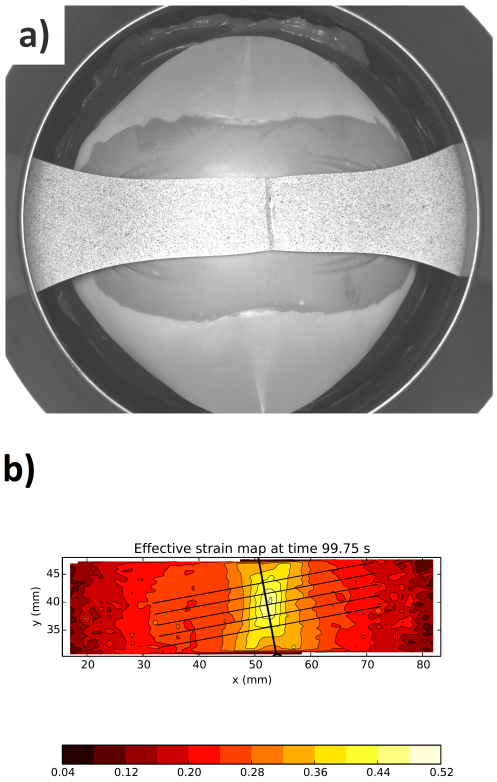

Figure 6: Standard method used for NK0-100-1 sample: (a) sample view, (b) strain map with cross-section lines and (c) strain distribution

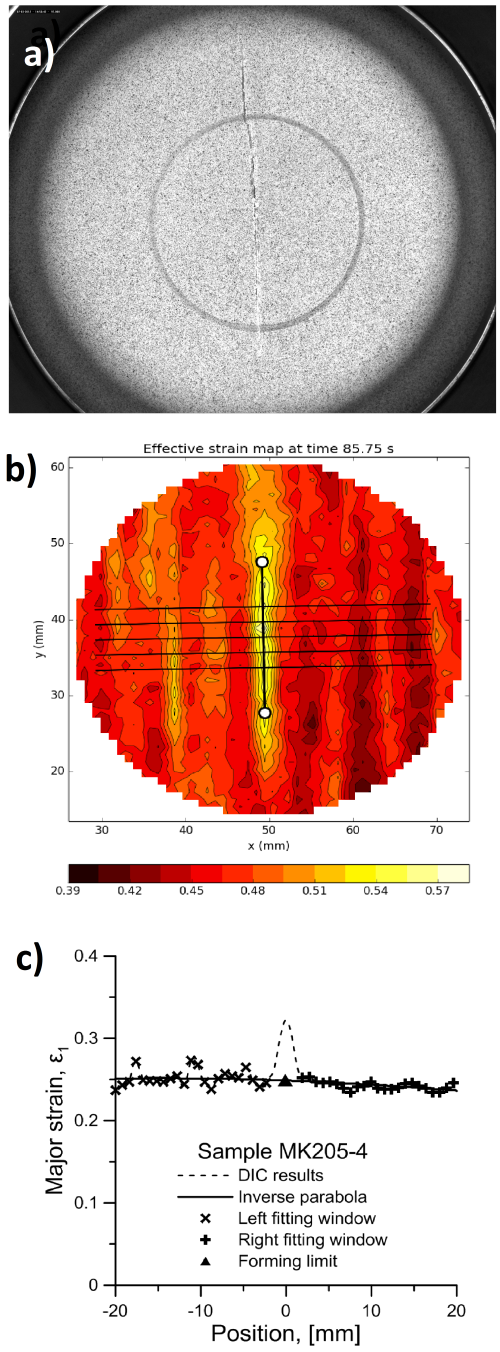

Figure 7: Standard method used for MK205-4 sample: (a) sample view, (b) strain map with cross-section lines and (c) strain distribution

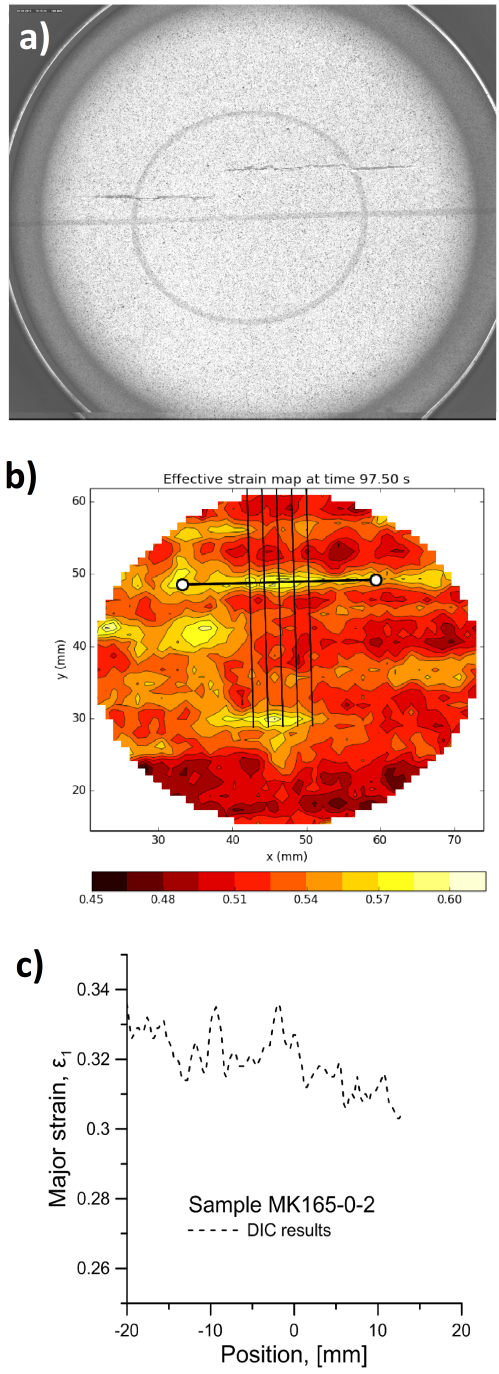

Figure 8: Standard method used for MK165-0-2 sample: (a) sample view, (b) strain map with cross-section lines and (c) strain distribution

Figure 9: Roping and multiple local necks in an Marciniak-Kuczynski sample

an alternative method for the detection of forming limit strain had to be developed to determine the forming limit strains in a user-independent, robust and repeatable manner. It was desirable to test the method on a simpler case prior to applying it to the formability tests at hand. Uniaxial tension testing of strip-shaped specimens provided such a case, so the method was tried out on such tests prior to applying it to formability tests. This initial application was reported earlier by Vysochinskiy et al. (2014). In this article, we present the outline of the method and its application to formality tests.

4. Thickness-control method

The proposed method is based on the monitoring of the metal sheet thickness and hence is referred to as the thickness-control method. The detection of local necking is based on comparison of local and global deformation similarly to the Finite Element (FE) based FLC calculator used by Reyes et al. (2006) and further developed by Fyllingen et al. (2009). The main principles and outline of the method are presented below.

4.1. Evaluation radius

The method relies on the concept of an evaluation radius. Reyes et al. (2006) used an evaluation radius for the FE-based FLC calculator. In connection with DIC, the evaluation radius was first used by Merklein et al. (2010).

As mentioned above, the strain-rate based methods rely on analysis of the strain-rate history of a region affected by the local neck. In practice this region could be represented by a single element or facet in the DIC analysis. However, using a single element produces a noisy curve which is difficult to analyse. Using an average over a group of elements cancels out some of the random noise and produces a smoother curve. A straightforward way to define this group of elements is to consider all the elements within a given radius from the material point of interest. This defines the concept of an evaluation radius.

In our implementation, the evaluation radius is determined in the reference configuration, i.e. it designates a fixed set of elements. The averages of internal parameters are then calculated over this fixed set.

In the proposed method the concept of an evaluation radius is exploited further. We define not one, but two evaluation radii. A small one to characterize the deformation of a region inside the local neck and a large one to describe the deformation of the surrounding area. The parameters obtained using the small evaluation radius have superscript *point* while the parameters obtained using the large evaluation radius have superscript *area*, e.g. ϵ_1^{point} and ϵ_1^{area}. For the example samples NK0-100-1, MK205-4 and MK165-0-2 the areas denoted by r^{point} and r^{area} are illustrated in Fig. 10(a), 11(a) and 12(a), respectively. The corresponding plots of the major strain-rate history are given in Fig. 10(b), 11(b) and 12(b) to illustrate how a larger evaluation radius produces a smoother curve.

4.2. Thickness ratio

The onset of local necking is characterized by rapid local thinning. Thus, a comparison of the sheet thickness in the material point of interest with the

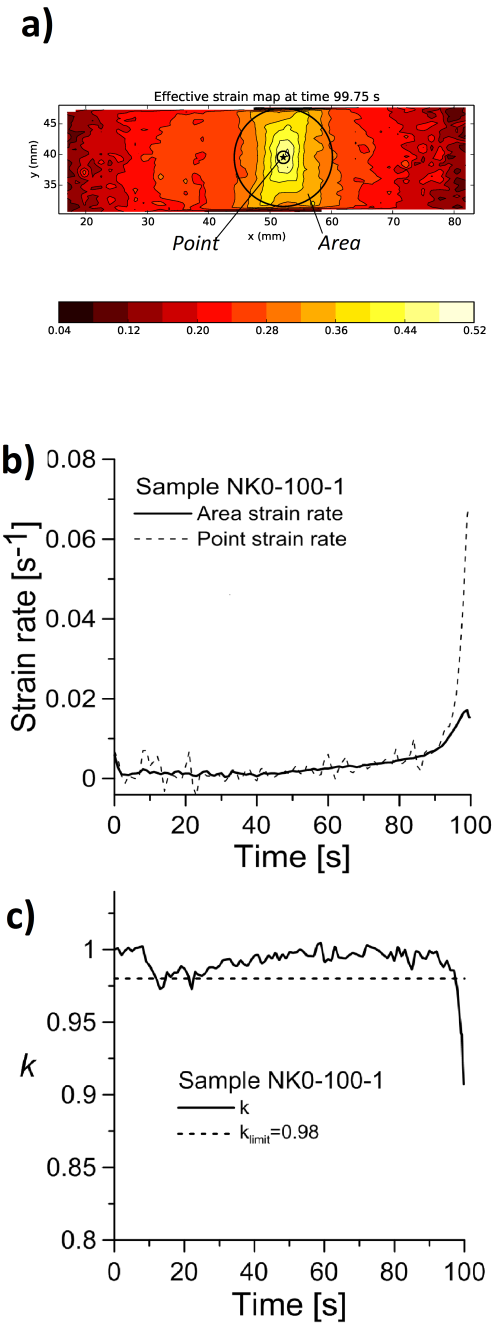

Figure 10: NK0-100-1 sample: (a) evaluation areas, (b) major strain rate evolution and (c) thickness ratio evolution

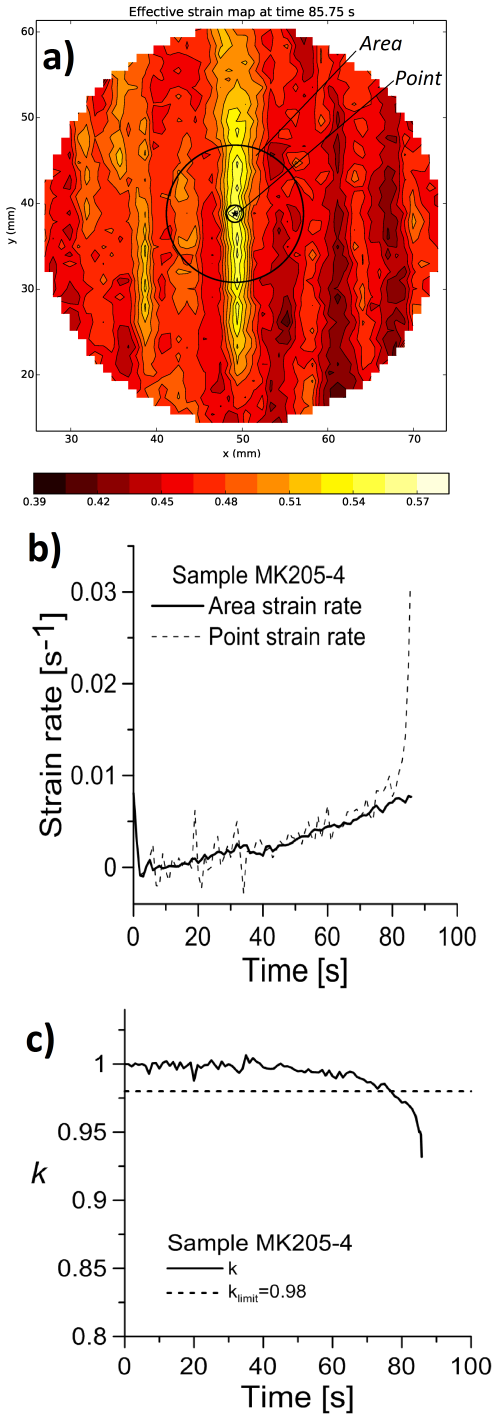

Figure 11: MK205-4 sample: (a) evaluation areas , (b) major strain rate evolution and (c) thickness ratio evolution

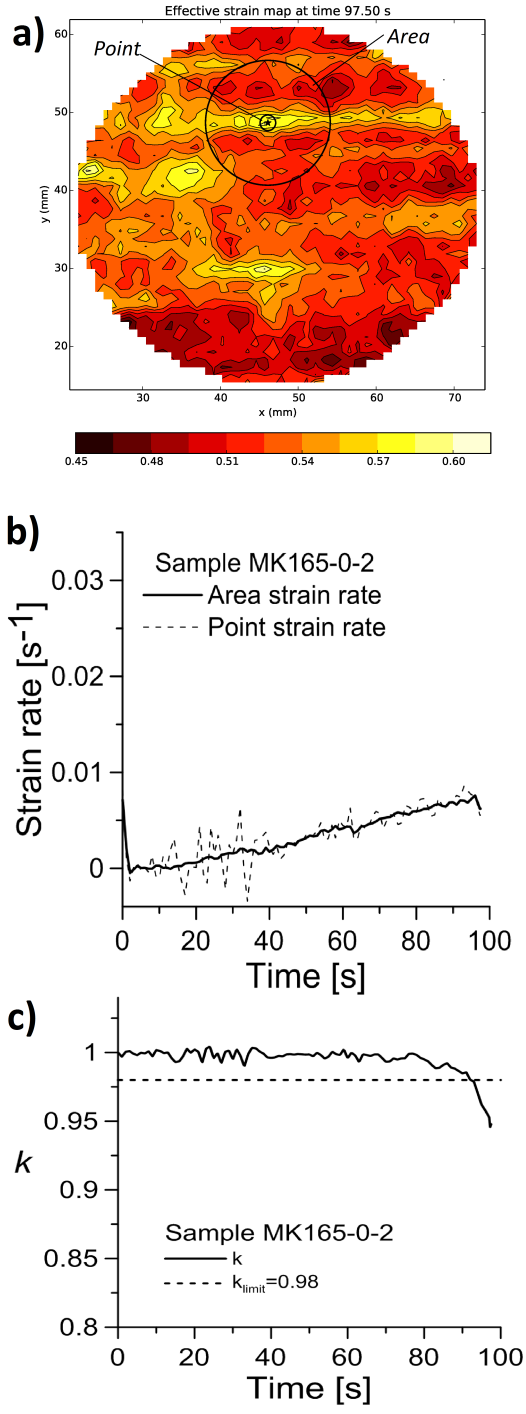

Figure 12: MK165-0-2 sample: (a) evaluation areas , (b) major strain rate evolution and (c) thickness ratio evolution

average thickness over the surrounding area can be a direct indicator of the onset of local necking.

Let us define a thickness ratio k as

$$k = \frac{t^{point}}{t^{area}} \tag{1}$$

where t^{point} is the point thickness, i.e. the sheet thickness determined using the small evaluation radius, and t^{area} is the area thickness, i.e. the sheet thickness determined using the larger evaluation radius. The ratio k equals unity when the strain field within the larger evaluation radius is uniform, and will start to deviate from unity when the local necking starts.

The DIC analysis produces in-plane strains. It is traditional for metal forming to use the true principal strains ϵ_1 and ϵ_2. Let us express the thickness ratio k in terms of the traditional deformation measures. The value of k can be easily calculated as the ratio of principal stretches. The principal stretch in the thickness direction is defined as

$$\lambda_3 = \frac{t}{t_0} \tag{2}$$

where t_0 and t are the initial and current values of the sheet thickness respectively. The true strain in the thickness direction ϵ_3 is related to the principal stretch λ_3 as

$$\epsilon_3 = \ln \lambda_3 \tag{3}$$

The ratio k can be expressed as

$$k = \frac{t^{point}}{t^{area}} = \frac{t^{point}}{t_0}\frac{t_0}{t^{area}} = \frac{\lambda_3^{point}}{\lambda_3^{area}} \tag{4}$$

Constant volume is assumed for the metal sheets and implies that

$$\epsilon_1 + \epsilon_2 + \epsilon_3 = 0 \tag{5}$$

This allows us to express λ_3 as

$$\lambda_3 = \exp(\epsilon_3) = \exp(-\epsilon_1 - \epsilon_2) \tag{6}$$

and k as

$$k = \frac{\exp(-\epsilon_1^{point} - \epsilon_2^{point})}{\exp(-\epsilon_1^{area} - \epsilon_2^{area})} \tag{7}$$

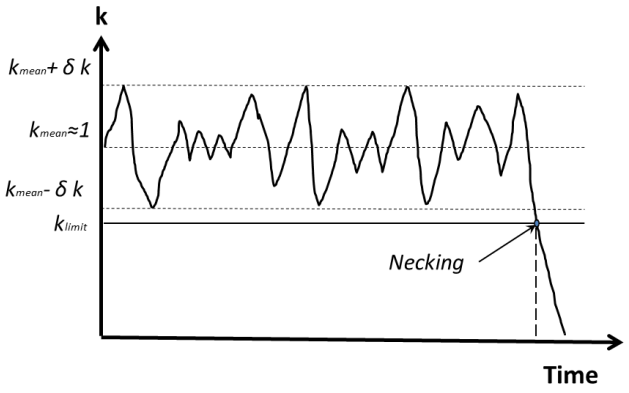

Figure 13: Detection of the onset of necking

4.3. Failure time and strains

In metal forming, there are two events that can be regarded as sheet failure: onset of local necking and fracture. The last time step of the DIC-analysis corresponds to the last image before fracture appears visible. This time step is considered to be the onset of fracture. Thus, the fracture time $\tilde{t}_{fracture}$ is assumed to be known a priori, while the time at the onset of local necking $\tilde{t}_{necking}$ needs to be determined.

In the case of globally homogeneous deformation, the thickness ratio k introduced above remains equal to unity up until the onset of local necking. There is some natural variation in the value of k due to the noise in the strain measurements. In addition, phenomena connected to locally inhomogeneous deformation, e.g. roping, might also contribute to the noise.

Let the value of δk denote the level of noise in the experimentally detected k vs. time curve and k_{mean} the time-average of k, as Fig. 13 illustrates. Let us also introduce a parameter $k_{limit} < k_{mean}$ that denotes the level of k at which the onset of local necking is detected, see Fig. 13. In order to detect the onset of local necking, the deviation of k from its mean value must exceed the level of noise δk. Therefore, the limitation $k_{limit} \leq k_{mean} - \delta k$ applies.

The value of δk can be estimated for each individual test from a statistical

analysis of k vs. time data. The value of k_{limit} is then set to fit all the tests.

If k drops below k_{limit} we conclude that onset of local necking is observed, while if this does not happen we conclude that no local necking was observed prior to fracture. Thus, we introduce an unambiguous and user-independent criterion to distinguish failure by local necking from direct failure by fracture.

Having determined the time of onset of local necking we can determine the corresponding failure strains. Prior to the onset of local necking, the area and point strains are supposed to be equal in the case of homogeneous deformation, i.e. $\epsilon_i^{area} \approx \epsilon_i^{point}$. The onset of local necking corresponds to a rapid increase of the local strains. Thus, using the area strain produces a smaller error in strain for the same error in time. In addition, when constructing an FLC, we are interested in the homogeneous strains that can be safely achieved. Therefore, we define the local necking strains as the area strains at the onset of local necking

$$\epsilon_i^{necking} = \epsilon_i^{area}(\tilde{t}_{necking}) \tag{8}$$

Contrary to the forming limit strains, the fracture strains are local strains. Thus, we define the fracture strains as the largest point strains achieved

$$\epsilon_i^{fracture} = \epsilon_i^{point}(\tilde{t}_{fracture}) \tag{9}$$

4.4. Step-by-step procedure

The step-by-step procedure for detection of forming limit strains in the thickness-control method is the following:

1. Perform DIC analysis
2. Export strain field data
3. Select a point on the fracture line
4. Define two evaluation radii
5. Calculate and plot k vs. time
6. Estimate δk
7. Define k_{limit}

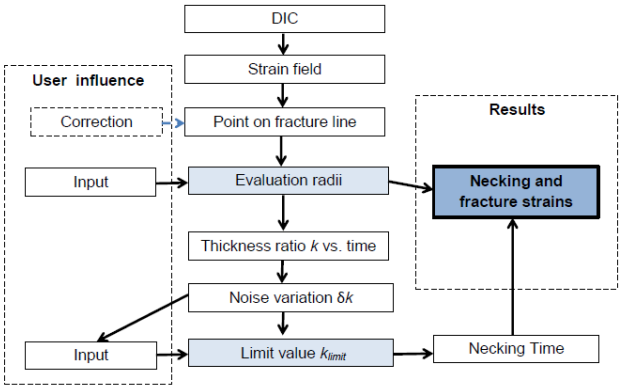

Figure 14: Thickness-control method outline

8. Determine whether or not local necking has taken place according to the k variation. If yes:
   (a) Determine $\tilde{t}_{necking}$
   (b) Determine local necking strains
9. Determine fracture strains

The procedure is illustrated in form of a flowchart in Fig. 14. Since the method was developed to minimize the effect of the user's judgement on the results, the points where the user might influence the outcome are given special attention.

The first point is the choice of a point on the fracture line, i.e. step 3. This step is semi-automatic with the initial automatic suggestion being the point that reached the highest effective (von Mises) strain. If this suggestion is off due to noise or other reasons, correction from the user is possible. Similarly, in the standard method, the user needs to specify the direction of the fracture. The second point is when the evaluation radii are defined, i.e. step 4 of the procedure. The third point is where the k_{limit} is decided, i.e. step 7 of the procedure. As was explained above, the choice of k_{limit} is not arbitrary, it is limited by the value of δk which might vary slightly from test to test. Choosing the same k_{limit} for all the tests allows to unify the procedure.

5. Application of the method

The method was initially tested on the uniaxial tension tests with 2D-DIC (Vysochinskiy et al., 2014). In these tests a single local neck was formed, thus a trial application allowed to verify that the method detects a physically sound onset of local necking. Here, the thickness-control method is applied to formability tests combined with 3D-DIC. The evaluation radii were set to 1 mm for point and 8 mm for area characteristics, respectively. The k_{limit} was set to 0.98 based on the estimate of δk by means of standard deviation and quantile range.

5.1. Nakajima tests

The majority of the tested Nakajima samples failed in the clamping zone. Only one geometry type produced three successful duplicate tests, namely the NK-100 samples that gave a strain-path between uniaxial tension and plane strain. These samples failed by the formation of a single local neck as illustrated in Fig. 6. Thus, both the thickness-control method and the standard method could be applied to these samples providing a comparison point.

Fig. 10 illustrates the application of the thickness-control method to one of these Nakajima samples. The onset of local thinning at the end of the test can be clearly observed in the k vs. time plot.

There are some features of the k vs. time plot that need to be commented upon. As can be seen in Fig. 10(c), k drops below k_{limit} at the beginning of the test. This drop was observed for all three duplicate tests and is likely to be connected to the punch curvature, i.e. to the effects of bending. Under the test, the initially flat Nakajima specimen assumes the shape of the spherical punch. Since DIC measures the strains on the surface of the specimen, the detected strains would be higher for the points that have assumed the punch shape in comparison with a yet flat region. This can lead to a falsely detected reduction of the sheet thickness at the point.

At the beginning of the test, prior to the contact of the specimen and the punch, the thickness ratio shall be constant. At this stage the whole specimen

remains flat. As the metal sheet at the point of interest starts to assume the spherical shape, the strains on its surface increase and k drops below k_{limit}. After a while, as the whole specimen assumes the shape of the punch, the difference between point and area strains disappears and k returns to being approximately equal to unity. All these stages are clearly observed in Fig. 10(c): at the first ten second of the tests k remains nearly constant, than a drop is observed after which k returns to being approximately unity at around 40 seconds.

The detected forming limit strain from the Nakajima tests are presented in Fig. 15. Each point represents one test. Both local necking and fracture strains are presented as well as the local necking strains determined by the the standard method and by the time-dependent method based on the algorithm of Merklein et al. (2010). For the standard method a single value for each sample is detected as an average of the five parallel cross-sections displayed in Fig. 6(b); the individual values for each cross section are also included in Fig. 15 to illustrate the scatter. It can be seen that the three methods detect forming limit strains significantly below fracture and with the similar level of scatter between the samples. The forming limits detected based on the algorithm of Merklein et al. (2010) appear to be the most conservative ones for this particular type of samples, while the thickness-control method is more conservative than the standard method. This is because both the time-dependent method and the thickness-control method detect the strains at the onset of local necking, while the standard method is based on the strains measured after the local neck is fully developed.

Fig. 16 illustrates the difference between the strain distribution for the time step at the onset of local necking used by the thickness-control method and the final time step used by the standard method.

5.2. Marciniak-Kuczynski tests

The k vs. time plots for the example samples MK205-4 and MK165-0-2 are shown in Fig. 11(c) and 12(c), respectively. In the Marciniak-Kuczynski tests

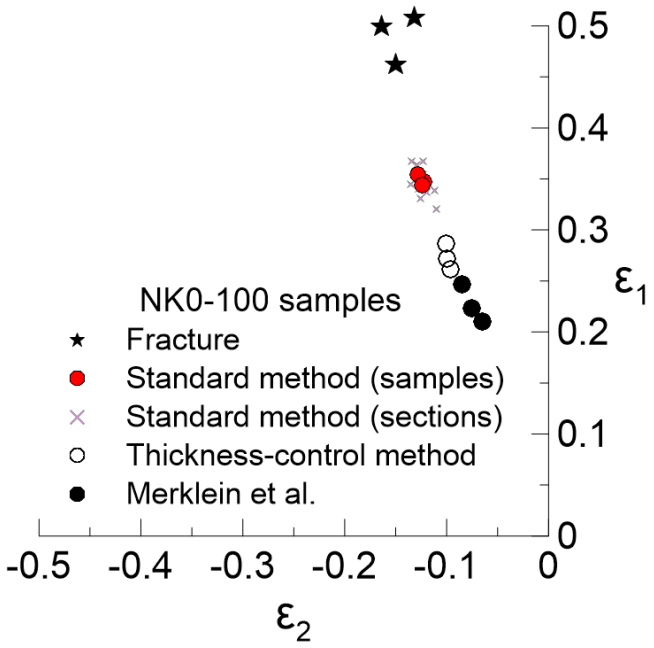

Figure 15: Comparison of the thickness-control method with the standard method and the time-dependent method of Merklein et al. (2010)

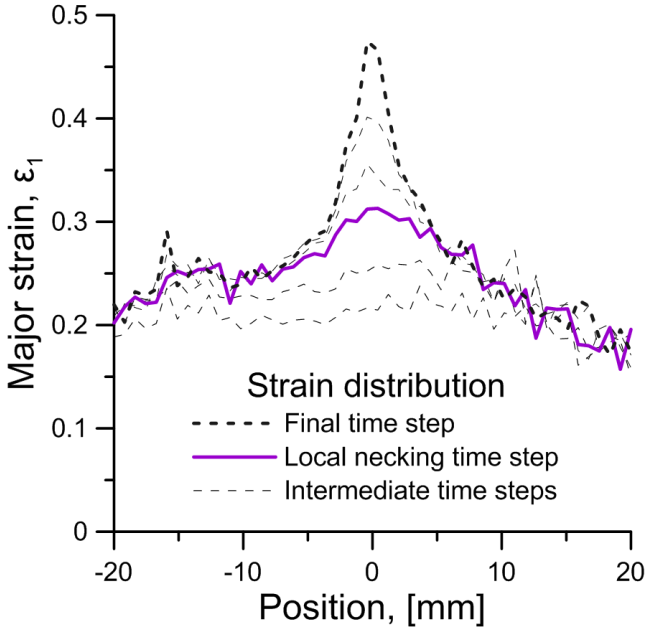

Figure 16: Strain distribution for different time steps

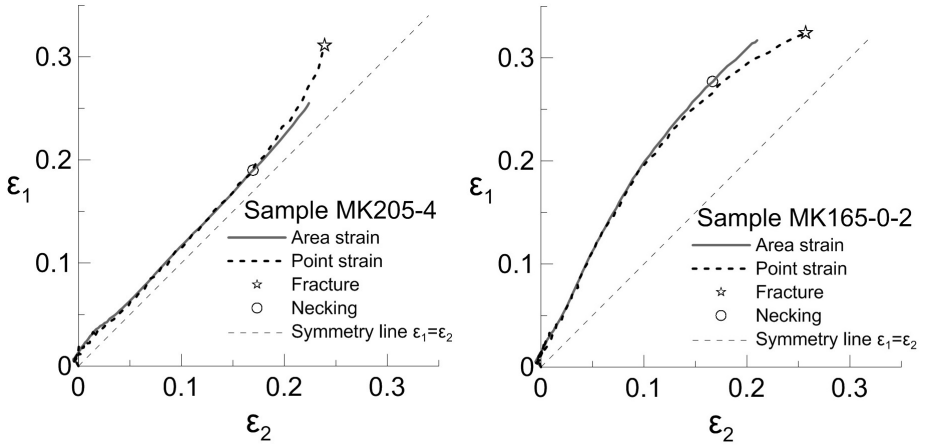

Figure 17: DIC-based strain paths for MK205-4 (left) and MK165-0-2 samples (right)

the area of interest remains flat so there are no bending effects on the presented plots. The subsequent detection of local necking and fracture strains for these samples are illustrated in Fig. 17 which presents the strain-paths obtained for MK205-4 and MK165-0-2 with marked fracture and local necking strains.

The "anomalous" orientation of the local neck and fracture line parallel to the major strain in MK165-0-2 sample leads to some interesting observations. Analysis of the k vs. time plot in Fig. 12 indicates that local thinning is observed and thus that local necking occurred prior to fracture. The strain maps in Fig. 8 also suggest occurrence of multiple local necks. But, due to the "anomalous" fracture orientation, the local neck formation causes increase not in the major strain ϵ_1, but in the minor strain ϵ_2, as can be seen in Fig. 17. Thus, no sudden increase in the major strain rate $\dot{\epsilon}_1$ is observed for this sample (see Fig. 12).

The use of the thickness-control method allowed to detect forming limit strains for all the tested Marciniak-Kuczynski samples. The results are summarized in Fig. 18 where each point represents one test sample, ϵ_{RD} is the true strain in the rolling direction and ϵ_{TD} is the true strain in the transverse direction.

Fig. 19 includes a comparison of the obtained FLC with the standard method and the time-dependent method of Merklein et al. (2010). Note that to produce

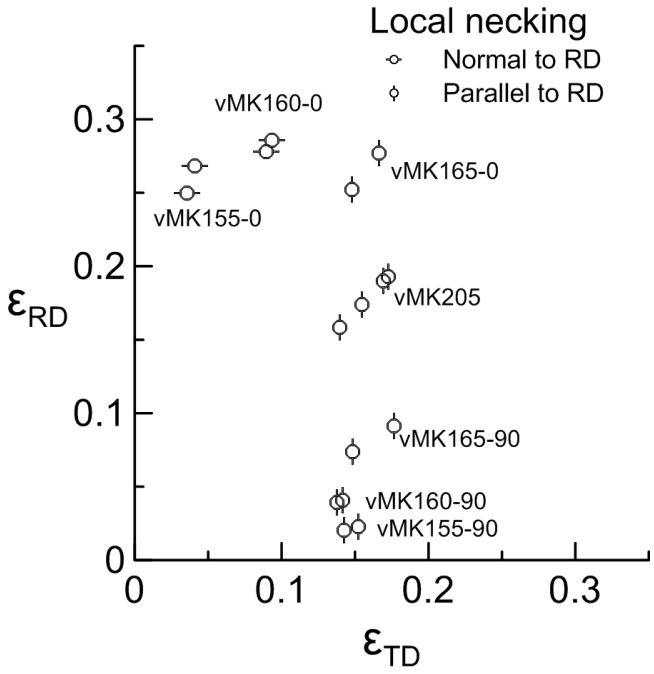

Figure 18: Forming limit strains detected by the thickness-control method

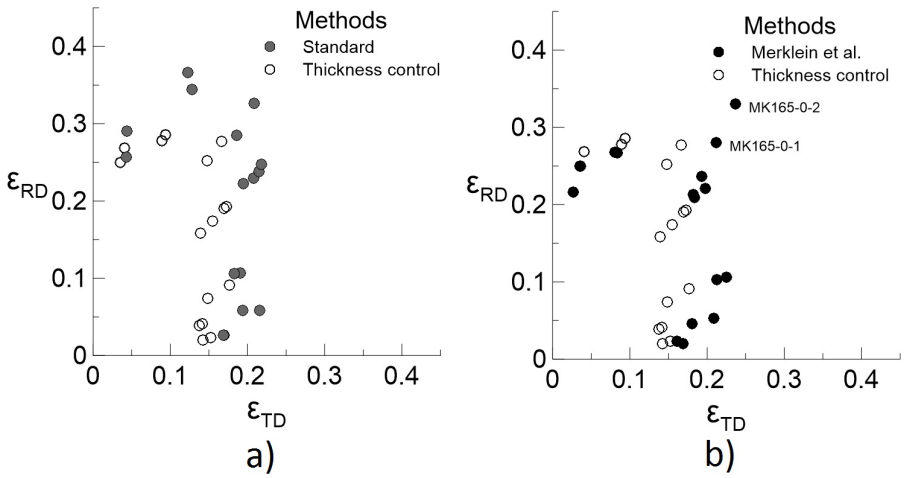

Figure 19: Thickness-control method compared to (a) the standard method and (b) the time-dependent method of Merklein et al. (2010)

plot at Fig. 19(a) the requirement to discard samples with multiple local necks (ISO12004-2:2008, 2008) had to be ignored. As can be seen in Fig. 19(a), the thickness-control method is more conservative than the standard method in the whole biaxial stretching region. From Fig. 19(b) we can see that the time-dependent method (Merklein et al., 2010) is more conservative than the thickness-control method when the major strain is along the RD, while the opposite is true when the major strain is along the TD. The largest deviation between the thickness-control method and method of Merklein et al. (2010) is observed for the MK165-0 type samples. As explained earlier, in these samples the local necks form parallel to the major strain due to roping effect. Hence, no sudden increase of the major strain rate is observed.

5.3. Sensitivity study

As indicated in Fig. 14, apart from the occasional correction of the fracture point location, the only points where the input from the user affects the result in the thickness-control method are the choice of the evaluation radii and k_{limit}.

The parameter k_{limit} has a clear physical meaning. It denotes the allowable degree of local thinning before local necking is considered to be detected. Thus,

the effect of variation of this parameter is trivial. The more thinning is allowed, the closer the detected forming limit strains would be to the fracture strains. For accurate detection of the local necking strains k_{limit} needs to be set as close to unity as the level of noise δk allows.

To investigate the effect of the variation of r^{area} and r^{point}, a sensitivity study was performed. The forming limit strains were detected using the same $k_{limit} = 0.98$ while different combinations of the area and point evaluation radii were used. Fig. 20 illustrates the effect of various values of r^{area} on the detected forming limits strains. In the Nakajima tests the use of larger values of r^{area} leads to smaller limit strains detected, while no such effect is observed for the Marciniak-Kuczynski tests. This is to be expected since in Nakajima tests use of a spherical punch creates a strain gradient with larger strains near the top of the punch (see Fig. 10(b)). Thus, use of larger evaluation radius produces a smaller average strain and more conservative results. No such effect is observed in the Marciniak-Kuczynski tests where a flat punch is used. For these tests the only effect of the larger area radius is a slight reduction of the scatter.

Predictably, keeping the same k_{limit} and r^{area} while changing r^{point} causes the onset of necking to be detected earlier for the smaller r^{point} and later for the larger r^{point}, as Fig. 21 illustrates.

6. Discussions and Conclusions

A new DIC-based method for detection of forming limit strains is proposed. The initial motivation for developing the method was the need to detect forming limit strains in samples that experienced multiple strain localizations, but the application of the method is not limited to this particular case. The developed thickness-control method is universal and can be used when a single local neck is formed or even when the samples fail directly by fracture without local neck formation. Furthermore, the method can be used in combination with different formability tests.

In the proposed thickness-control method, the onset of local necking is con-

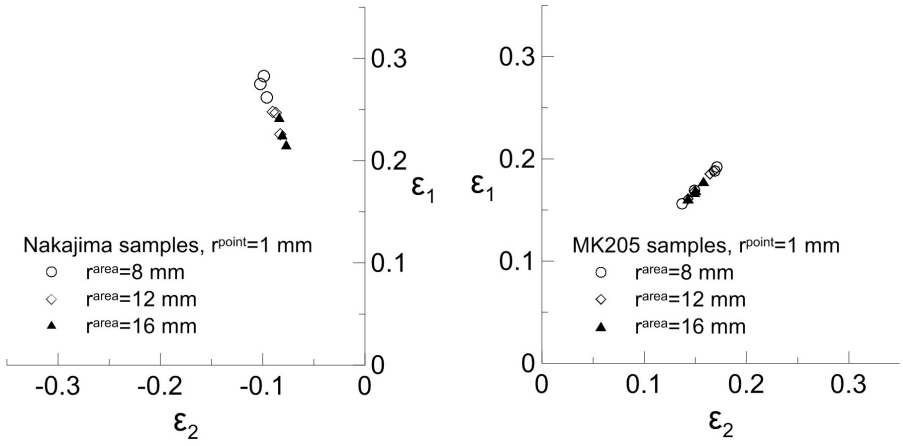

Figure 20: Thickness-control method: effect of r^{area} variation for Nakajima (left) and Marciniak-Kuczynski tests (right)

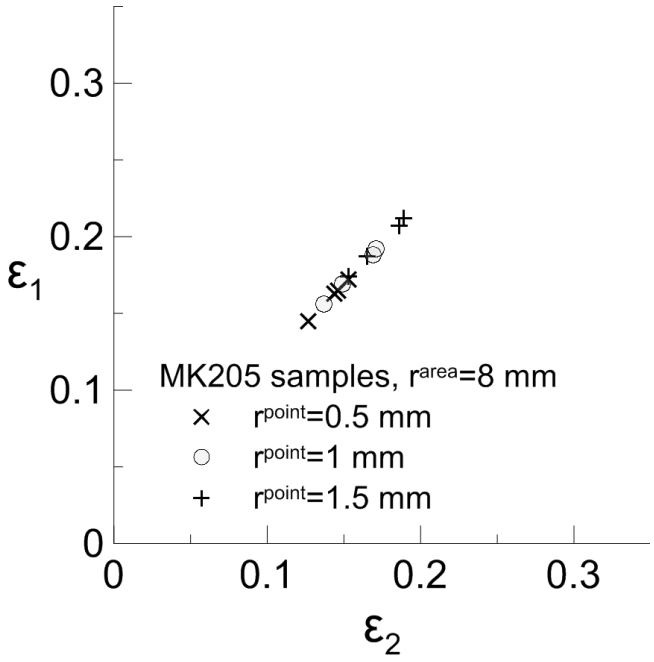

Figure 21: Thickness-control method: effect of varying r^{point}

sidered to occur when the local thinning exceeds the allowable tolerance. Thus, the criterion for onset of local necking has a clear physical meaning. As illustrated in Fig. 14, the detection of the forming limits is automated and the only way the user influences the results is through the input parameters r^{point}, r^{area} and k_{limit}, where r^{point} denotes the area over which the local thickness is measured, r^{area} denotes the area over which the average thickness is measured and k_{limit} denotes the degree of thinning at which the local necking is detected.

In order to detect the forming limit strains with maximum accuracy it is desirable to set r^{point} as small as possible, r^{area} as large as possible and k_{limit} as close to unity as possible, but these parameters have physical constraints: r^{point} is limited by the size of an element in the DIC analysis, r^{area} is limited by the size of the homogeneously deformed part of the sample and k_{limit} is limited by the level of the noise δk. These constraints might be different for different laboratories that use various DIC software and test set-ups. Using the thickness-control method with the same combination of r^{point}, r^{area} and k_{limit} allows to obtain quantitatively comparable results.

The comparison of the standard (ISO12004-2:2008, 2008) and the thickness-control methods revealed that both methods demonstrate the same level of scatter between samples, but the thickness-control method produces a more conservative estimate of the forming limit strains. In the thickness-control method it is possible to produce less conservative results by simply lowering k_{limit}, i.e. by increasing the allowable degree of thinning. Thus, if desired, it is possible to construct several FLCs applying different k_{limit}. This approach would be similar to the LL-FLD method proposed by Hora et al. (2012), where different levels of strain localization are used to construct several FLCs. In the future, it might be possible to standardize the input parameters and link different levels of strain localization to different levels of local thinning.

Acknowledgements

The presented research is conducted in a course of the Ph.D. study at the Norwegian University of Technology, Trondheim, Norway. The AA6016 sheets were supplied by the industrial partner Hydro Aluminium Rolled Products GmbH, Bonn, Germany.

References

Engler, O., Schäfer, C., & Brinkman, H.-J. (2012). Crystal-plasticity simulation of the correlation of microtexture and roping in AA 6xxx Al-Mg-Si sheet alloys for automotive applications. *Acta Materialia*, *60*, 5217–5232. URL: http://linkinghub.elsevier.com/retrieve/pii/S1359645412004119. doi:10.1016/j.actamat.2012.06.039.

Fyllingen, O., Hopperstad, O., Lademo, O., & Langseth, M. (2009). Estimation of forming limit diagrams by the use of the finite element method and Monte Carlo simulation. *Computers & Structures*, *87*, 128–139. URL: http://linkinghub.elsevier.com/retrieve/pii/S0045794908001703. doi:10.1016/j.compstruc.2008.07.002.

Goodwin, G. M. (1968). Application of strain analysis to sheet metal forming problems in the press shop. SAE Technical Paper 680093. doi:10.4271/680093.

Hora, P., Bekim, B., Gorji, M., & Manopulo, N. (2012). A generalized approach for the prediction of necking and rupture phenomena in the sheet metal forming. Proceedings of IDDRG 2012 (pp. 79–93).

Hosford, W. F., & Caddell, R. M. (2007). *Metal Forming*. (3rd ed.). Cambridge: Cambrige University Press.

Hotz, W., Merklein, M., Kuppert, A., Friebe, H., & Klein, M. (2013). Time dependent FLC determination - Comparison of different algorithms to detect the onset of unstable necking before fracture. *Key Engineering Materials*, *549*,

397–404. URL: http://www.scopus.com/inward/record.url?eid=2-s2.0-84877860298&partnerID=40&md5=d816078f3b842bec1db17ba4f83ad7a6.

ISO12004-2:2008, I. S. (2008). Metallic materials - Sheet and strip - Determination of forming-limit curves. Part 2: Determination of forming-limit curves in the laboratory.

Janssens, K., Lambert, F., Vanrostenberghe, S., & Vermeulen, M. (2001). Statistical evaluation of the uncertainty of experimentally characterised forming limits of sheet steel. *Journal of Materials Processing Technology*, *112*, 174 – 184. URL: http://www.sciencedirect.com/science/article/pii/S0924013600008906. doi:http://dx.doi.org/10.1016/S0924-0136(00)00890-6.

Keeler, S. P. (1968). Circular grid system – a valuable aid for evaluating sheet metal formability. SAE Technical Paper 680092. doi:10.4271/680092.

Liebertz, H., Duwel, A., Illig, R., Hotz, W., Keller, S., Koehler, A., Kröff, A., Merklein, M., Rauer, J., Staubwasser, L., Steinbeck, G., & Vegter, H. (2004). Guideline for the Determination of Forming Limit Curves. In *Proceedings of International Deep Drawing Research Group (IDDRG) Conference*. Sindelfingen, Germany.

Marciniak, Z., & Kuczynski, K. (1967). Limit strains in the processes of stretch-forming sheet metal. *International Journal of Mechanical Sciences*, *9*, 609–620.

Marron, G., Moinier, L., Patou, P., & Celeski, J. (1997). A new necking criterion for forming limit diagrams. In *Proceedings of the International Deep Drawing Research Group 1997 WG Meeting, Haugesund*.

Merklein, M., Kuppert, A., & Geiger, M. (2010). Time dependent determination of forming limit diagrams. *CIRP Annals - Manufacturing Technology*, *59*, 295–298. URL: http://linkinghub.elsevier.com/retrieve/pii/S0007850610000028. doi:10.1016/j.cirp.2010.03.001.

Nakajima, K., Kikuma, T., & Hasuka, K. (1968). *Study of the formability of steel sheets*. Technical Report Technical Report No. 264, 8517-8530 Yawata.

Reyes, A., Hopperstad, O., Lademo, O., & Langseth, M. (2006). Modeling of textured aluminum alloys used in a bumper system: Material tests and characterization. *Computational Materials Science*, *37*, 246–268. URL: http://linkinghub.elsevier.com/retrieve/pii/S0927025605002582. doi:10.1016/j.commatsci.2005.07.001.

Situ, Q., Jain, M., & Metzger, D. (2011). Determination of forming limit diagrams of sheet materials with a hybrid experimentalnumerical approach. *International Journal of Mechanical Sciences*, *53*, 707 – 719. URL: http://www.sciencedirect.com/science/article/pii/S0020740311001135. doi:http://dx.doi.org/10.1016/j.ijmecsci.2011.06.003.

Vacher, P., Dumoulin, S., Morestin, F., & Mguil-Touchal, S. (1999a). Bidimensional strain measurement using digital images. *Proceedings of the Institution of Mechanical Engineers, Part C: Journal of Mechanical Engineering Science*, *213*, 811–817. URL: http://pic.sagepub.com/lookup/doi/10.1243/0954406991522428. doi:10.1243/0954406991522428.

Vacher, P., Haddad, A., & Arrieux, R. (1999b). Determination of the forming limit diagrams using image analysis by the corelation method. {*CIRP*} *Annals - Manufacturing Technology*, *48*, 227 – 230. URL: http://www.sciencedirect.com/science/article/pii/S0007850607631710. doi:http://dx.doi.org/10.1016/S0007-8506(07)63171-0.

Volk, W., & Hora, P. (2011). Evaluation of Experimental Forming Limit Curves and Investigation of Strain Rate Sensitivity for the Start of Local Necking. In *The 8th International Conference and Workshop on Numerical Simulation of 3D Sheet Metal Forming Processes* (pp. 99–106). volume 106. URL: http://link.aip.org/link/APCPCS/v1383/i1/p99/s1&Agg=doi. doi:10.1063/1.3623598.

Vysochinskiy, D. (2014). *Formability of aluminium alloy subjected to prestrain by rolling*. Ph.D. thesis Norwegian University of Science and Technology. URL: http://hdl.handle.net/11250/275620.

Vysochinskiy, D., Coudert, T., Hopperstad, O. S., Lademo, O.-G., & Reyes, A. (2014). Experimental detection of the onset of local necking in an aluminium sheet. *Materials Science Forum*, *796*, 590–595. doi:10.4028/www.scientific.net/MSF.794-796.590.

Vysochinskiy, D., Coudert, T., Reyes, A., & Lademo, O. G. (2012). Determination of Forming Limit Strains Using Marciniak-Kuczynski Tests and Automated Digital Image Correlation Procedures. *Key Engineering Materials*, *504-506*, 17–22. URL: http://www.scientific.net/KEM.504-506.17.

Wang, K., Carsley, J. E., He, B., Li, J., & Zhang, L. (2014). Measuring forming limit strains with digital image correlation analysis. *Journal of Materials Processing Technology*, *214*, 1120 – 1130. URL: http://www.sciencedirect.com/science/article/pii/S0924013614000119. doi:http://dx.doi.org/10.1016/j.jmatprotec.2014.01.001.